

A Coupled Theory of Tropical Climatology: Warm Pool, Cold Tongue, and Walker Circulation

ZHENGYU LIU AND BOYIN HUANG

Department of Atmospheric and Oceanic Sciences, University of Wisconsin—Madison, Madison, Wisconsin

(Manuscript received 1 November 1995, in final form 12 September 1996)

ABSTRACT

Based on results from analytic and general circulation models, the authors propose a theory for the coupled warm pool, cold tongue, and Walker circulation system. The intensity of the coupled system is determined by the coupling strength, the local equilibrium time, and latitudinal differential heating. Most importantly, this intensity is strongly regulated in the coupled system, with a saturation level that can be reached at a modest coupling strength. The saturation west–east sea surface temperature difference (and the associated Walker circulation) corresponds to about one-quarter of the latitudinal differential equilibrium temperature. This regulation is caused primarily by the decoupling of the SST gradient from a strong ocean current. The author's estimate suggests that the present Pacific is near the saturation state. Furthermore, the much weaker Walker circulation system in the Atlantic Ocean is interpreted as being the result of the influence of the adjacent land, which is able to extend into the entire Atlantic to change the zonal distribution of the trade wind. The theory is also applied to understand the tropical climatology in coupled GCM simulations, in the Last Glacial Maximum climate, and in the global warming climate, as well as in the regulation of the tropical sea surface temperature.

1. Introduction

A striking feature of the tropical Pacific and Atlantic annual mean sea surface temperature (SST) is a warm pool in the west and a cold tongue in the east. Accompanied with this warm pool–cold tongue SST pattern is a Walker circulation in the atmosphere, which ascends above the west and descends over the east (Bjerknes 1969; Flohn 1971; Newell 1979). From the viewpoint of a coupled ocean–atmosphere system, the warm pool, cold tongue, and Walker circulation system (WCWC) can be forced by the Hadley circulation, whose equatorward converging surface wind is deflected by the Coriolis force toward the west, and therefore causes upwelling and, in turn, the cold tongue in the east (e.g., McWilliams and Gent 1978, hereafter MG). The WCWC can also be established by the ocean–atmosphere positive feedback between the upwelling and easterly wind—the so-called climatological version of Bjerknes hypothesis (Neelin and Dijkstra 1995; Dijkstra and Neelin 1995, hereafter ND). However, the mechanism that determines the intensity of the WCWC in a coupled ocean–atmosphere system has not yet been studied. This will be the focus of this paper.

Given that the only external forcing to the climate

system is the solar radiation that is zonally uniform, several fundamental issues concerning the WCWC remain open. First, why is the present zonal SST difference about 4°C across the tropical Pacific? Why has this SST gradient seemed to have increased in the Last Glacial Maximum (LGM, CLIMAP 1976), but decreased in the CO₂ warming GCM experiments (Knutson and Manabe 1995; Meehl and Washington 1996)? Second, a recent intercomparison of a dozen fully coupled GCMs shows a puzzling feature (Fig. 1 of Mechoso et al. 1995): in spite of the dramatically different absolute SSTs on the equator, the zonal SST gradient along the equator shows a surprising agreement among all the models (except in the coastal region where the land effect is believed to be strong). Does this imply a saturation of the Pacific SST gradient that is independent of the absolute equatorial SST? If so, what determines the saturation level? Third, the observed zonal SST difference in the tropical Atlantic is no larger than 2°C. This leads to the question, why is the WCWC so different between the Atlantic and the Pacific?

A coupled theory is presented here for the WCWC system. Special attention will be paid to the mechanism that determines the intensity of the WCWC in a coupled system. A distinctive feature of our work is the explicit inclusion of the extratropics in the combined tropical–extratropical coupled ocean–atmosphere system. It will be shown that the intensity of WCWC is regulated by an upper bound, or saturation level, which is equivalent to about one-quarter of the equilibrium SST difference

Corresponding author address: Dr. Zhengyu Liu, Dept. of Atmospheric and Oceanic Sciences, University of Wisconsin—Madison, 1225 W. Dayton Street, Madison, WI 53706-1695.
E-mail: znl@ocean.meteor.wisc.edu

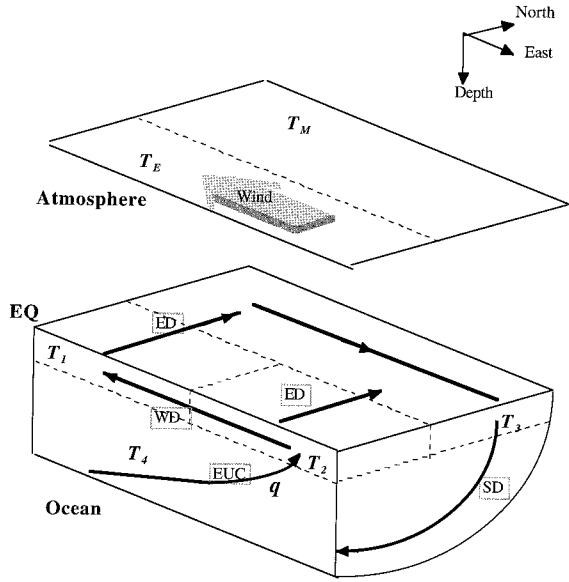


FIG. 1. Schematic figure for the four-box ocean model. The surface Pacific equator is represented by surface western and eastern boxes, with the temperatures of T_1 and T_2 , respectively. The surface midlatitude ocean is represented by the third box with the temperature of T_3 . The midlatitude thermocline is combined with the equatorial thermocline as a thermocline box with a temperature of T_4 . Major ocean currents are labeled as EUC for equatorial undercurrent and upwelling, WD for surface westward wind drift, ED for poleward Ekman drift, and SD for subtropical subduction flow.

between the Tropics and the midlatitudes. Furthermore, the saturation is caused by the decoupling of the SST gradient from the ocean dynamics in the presence of strong ocean currents. This saturation level would be dramatically overestimated, according to previous works, because of the neglect of either the local air–sea thermodynamic interaction (MG) or the zonal oceanic advection (ND). Our present saturation level puts the Pacific near the saturation state. The theory will also be shown to have some important implications for the role of ocean circulation in the tropical climatology.

To highlight the physical mechanism, we will adopt a conceptual model for the atmosphere. The ocean will be first studied with a simple box model and later with a general circulation model. The paper is arranged as follows. The coupled box model is introduced in section 2. The coupled dynamics of WCWC are studied in section 3. Supporting OGCM experiments are presented in section 4. The role of the Hadley circulation is discussed in section 5. The WCWC in the Atlantic is discussed in section 6. A summary and further discussions are given in section 7.

2. The coupled box model

a. The model

We first simulate the tropical–subtropical upper ocean with four boxes (Fig. 1): boxes 1, 2, 3, and 4, repre-

senting the surface warm pool, the cold tongue, and the extratropical surface and subsurface thermocline waters, respectively. The temperatures of the four boxes will be represented by T_1^* , T_2^* , T_3^* , and T_4^* . One important feature that distinguishes our ocean model from previous works (MG; ND) is the explicit consideration of a tropical–subtropical oceanic bridge. This oceanic bridge consists of the surface wind drift from the cold tongue toward the warm pool, the surface Ekman drift from the Tropics toward the extratropics, the subduction from the extratropical surface ocean toward the equator through the subsurface thermocline, and the equatorial undercurrent that upwells in the cold tongue. This circulation feature is well supported by observations (Fine et al. 1981; Fine et al. 1987; Toggweiler et al. 1989; Tsuchiya et al. 1989) and recent modelings (Pedlosky 1987; Liu 1994; Liu et al. 1994; McCreary and Lu 1994; Liu and Philander 1995).

The heat budget of each box is determined by the local surface heat flux and oceanic heat transports. Following the circulation in Fig. 1, we have

$$m_1 \frac{d}{dt} T_1^* = m_1 H_1 + (1 - \epsilon)q(T_2^* - T_1^*), \quad (2.1a)$$

$$m_2 \frac{d}{dt} T_2^* = m_2 H_2 + q(T_4^* - T_2^*), \quad (2.1b)$$

$$m_3 \frac{d}{dt} T_3^* = m_3 H_3 + \epsilon q(T_2^* - T_3^*) + (1 - \epsilon)q(T_1^* - T_3^*), \quad (2.1c)$$

$$m_4 \frac{d}{dt} T_4^* = q(T_3^* - T_4^*), \quad (2.1d)$$

where m_i ($i = 1, 2, 3, 4$) is the volume of each box and H_i ($i = 1, 2, 3$) is the surface heat flux for each surface box. The net upwelling transport, after proper dimensionalization, is q , of which ϵq and $(1 - \epsilon)q$ leak out from the eastern and western boxes, respectively, into the extratropics due to the Ekman drift.

Considering the thermodynamic ocean–atmosphere coupling, the surface air–sea heat flux will be approximated as a restoring toward the local equilibrium SSTs with a restoring time τ_r . That is,

$$H_1 = (T_E - T_1)/\tau_r, \quad H_2 = (T_E - T_2)/\tau_r, \\ H_3 = (T_M - T_3)/\tau_r. \quad (2.2)$$

Here, T_E and T_M (with $T_E > T_M$) are the equilibrium SSTs in the Tropics and the midlatitudes, respectively. They represent the effective latitudinal differential heating that is the only external forcing to the coupled system. (The equilibrium SST here represents the SST that will be reached in the absence of ocean currents.) The restoring time τ_r is a measure of the intensity of local air–sea negative feedback. Considering the atmospheric radiation feedback and the large-scale nature of the WCWC system (Bretherton 1982; Lau and Nath 1996;

Sun and Liu 1996), the restoring time should be much longer than 30 days (Haney 1971) in a mixed layer of 50 m. Here, a typical value is taken as about $\tau_r = 200$ days.

The ocean transport q is the net upward transport into the eastern equatorial box, which also represents the net exchange transport between the tropical and subtropical ocean. This exchange transport is determined mainly by the Ekman transport (Liu 1994; Liu et al. 1994; McCreary and Lu 1994), which is proportional to the surface zonal wind stress τ^x . The wind stress is approximated to be proportional to the surface wind U , which is contributed by both the Hadley (U_H) and Walker (U_W) circulations. The Hadley and Walker circulations will be assumed to be driven by the meridional and zonal SST gradients (e.g., MG).¹ Thus,

$$q = a_1 \tau^x, \quad \tau^x = a_2 U,$$

$$U = U_H + U_W = a_H(T_{EQ}^* - T_3^*) + a_W(T_1^* - T_2^*), \quad (2.3a)$$

where $T_{EQ}^* = 0.5(T_1^* + T_2^*)$ is the mean equatorial SST. The coefficients a_1 , a_2 , a_H , and a_W are determined by the boundary layer processes and ocean–atmosphere interaction. Equation (2.3a) can be combined to give an ocean current that is generated by the dynamic ocean–atmosphere coupling as

$$q = A_H^*(T_{EQ}^* - T_3^*) + A_W^*(T_1^* - T_2^*) \geq 0. \quad (2.3b)$$

We will call $A_H^* = a_1 a_2 a_H$ and $A_W^* = a_1 a_2 a_W$ the Hadley and Walker coupling parameters respectively, which represent the dynamic coupling between the meridional and zonal SST gradients with the Hadley and Walker circulations, respectively. Our convention for the positive ocean current is in the direction shown in Fig. 1. Equations (2.1)–(2.3) form our coupled model. Notice that dynamic waves are filtered out in (2.1). This can be thought as the fast-wave limit (Neelin 1991). More importantly, it enables us to focus on the mean climatology, which seems to be determined more by the slow advective process in the tropical–subtropical ocean.

The model variables will be nondimensionalized as $T_i = (T_i^* - T_M)/(T_E - T_M)$; $i = 1, 2, 3, 4$; $Q = q\tau_r/m_1$; and $\tau = t/\tau_r$. Box 1 and box 2 are assumed to be of the same volume or $m_1 = m_2$. Combining (2.1) with (2.2), we have the nondimensional equations for the ocean as

$$\frac{d}{dt}T_1 = 1 - T_1 + (1 - \epsilon)Q(T_2 - T_1), \quad (2.4a)$$

$$\frac{d}{dt}T_2 = 1 - T_2 + Q(T_3 - T_2), \quad (2.4b)$$

and

$$m \frac{d}{dt}T_3 = -mT_3 + \epsilon Q(T_2 - T_3) + (1 - \epsilon)Q(T_1 - T_3), \quad (2.4c)$$

where $m = m_3/m_1$. For simplicity, $m_4 = 0$ has been used, and therefore $T_4 = T_3$. This reduces the four-box model to a three-surface-box model, with the thermocline box effectively being a zero volume pipe. This assumption does not change the steady-state solution, which is the focus of the present paper.

The dimensionless form of the transport (2.3b) is

$$Q = Q_H + Q_W \geq 0, \quad (2.5a)$$

where

$$Q_H = A_H(T_{EQ} - T_3), \text{ and } Q_W = A_W(T_1 - T_2). \quad (2.5b)$$

Here, A_H and A_W are the nondimensional Hadley and Walker coupling parameters

$$A_H = \tau_r A_H^*(T_E - T_M)/m_1 \equiv \tau_r/\tau_{aH}, \quad (2.5c)$$

and

$$A_W = \tau_r A_W^*(T_E - T_M)/m_1 \equiv \tau_r/\tau_{aW}, \quad (2.5d)$$

where

$$\tau_{aH} \equiv m_1/[A_H^*(T_E - T_M)] = (L/u_H)[\Delta_y T/(T_E - T_M)],$$

and

$$\tau_{aW} \equiv m_1/[A_W^*(T_E - T_M)] = (L/u_W)[\Delta_x T/(T_E - T_M)].$$

Here we have used L for the zonal width of box 1 or half the basin width, $u_H = q_H L/m_1$ ($u_W = q_W L/m_1$) for the Hadley- (Walker) driven zonal current speed, and $\Delta_y T$ ($\Delta_x T$) for the typical meridional (zonal) SST difference. Therefore, τ_H (τ_W) is the advection time for the Hadley- (Walker) driven surface current to cross half of the basin, were the SST difference in the meridional (zonal) direction the same as that of latitudinal equilibrium SST.

The dimensionless coupled system in Eqs. (2.4) and (2.5) is determined by four nondimensional parameters: ϵ , m , A_W , and A_H . Typical values for these parameters can be estimated for the Pacific as follows. Parameter ϵ is determined by the flow partitioning of the tropical–extratropical water exchange. All the water leaks to the extratropics through the western (eastern) box for $\epsilon = 0$ ($\epsilon = 1$). It will be called the branching parameter. Since most of the poleward Ekman flow should occur in the western part of the basin due to the westward surface wind drift, $\epsilon < 0.5$ seems to give a reasonable upper bound. Parameter m is the ratio of the volumes between the midlatitude ocean and half of the equatorial ocean, and therefore will be called the volume parameter. It seems reasonable to put $m \geq 1$ as a lower bound. The A_W and A_H will be estimated as follows. First, assume all of the trade wind to be caused by the Walker coupling (or $A_H = 0$). For typical values in the Pacific,

¹ A constant can be added to simulate the Hadley wind that is driven by the eddy (as in MG). Our results show that it will be similar to the meridional SST gradient effect.

$u = 25 \text{ cm s}^{-1}$, $L = 5000 \text{ km}$, $\Delta_x T = 4^\circ\text{C}$, and $T_E - T_M = 20^\circ\text{C}$; Eq. (2.5b) gives a τ_{aw} of about 50 days. This will give $A_w \approx 4$ if we take τ_r as 200 days. Then, we assume all of the trade wind to be generated by the Hadley coupling (or $A_w = 0$). For the Pacific, if we take $\Delta_y T = 12^\circ\text{C}$, we have a τ_{aH} about 150 days. This gives $A_H \approx 1.5$. In reality, both couplings exist. Thus, the estimated values can be treated as the upper bound—that is, roughly $A_H \leq 1.5$ and $A_w \leq 4$.

b. Solution

At steady state, the total heat conservation can be derived from (2.4) as

$$T_1 + T_2 + mT_3 = 2, \tag{2.6}$$

or $T_1^* + T_2^* + mT_3^* = 2T_E + mT_M$ in dimensional form. The steady-state solution can be obtained by first deriving the transport Q equation [from Eqs. (2.4) and (2.5)] as

$$B(Q)Q = A_w Q + A_H[(3/2 - \epsilon)Q + 1], \tag{2.7a}$$

where

$$B(Q) \equiv (1 + 2/m)(1 - \epsilon)Q^2 + (2 - \epsilon + 1/m)Q + 1. \tag{2.7b}$$

The zonal and meridional SST differences can then be derived from Eq. (2.4), as a function of Q , as

$$T_1 - T_2 = Q/B(Q) \tag{2.8a}$$

and

$$T_{EQ} - T_3 = [1 + (3/2 - \epsilon)Q]/B(Q). \tag{2.8b}$$

Equations (2.6)–(2.8) give the complete steady-state solutions. For a physically valid solution $Q \geq 0$, we have $B(Q) \geq 1$. Thus, the steady state satisfies $1 \geq T_1 \geq T_2 > T_3 \geq 0$. That is, the western equator will never be colder than the east equator, and both will always be warmer than the midlatitude ocean.

3. Coupled dynamics of WCWC

It is instructive to start our discussion without Hadley coupling ($A_H = 0$). Now, the transport equation (2.7a) collapses to two simpler equations:

$$Q = 0, \tag{3.1a}$$

and

$$B(Q) = A_w, \tag{3.1b}$$

where the latter is a quadratic equation. Furthermore, a substantial understanding can be gained by considering an even simpler case with $m = \infty$. This reduces (2.6) to

$$T_3 = 0, \tag{3.2}$$

or in dimensional form, $T_3^* = T_M$. The midlatitude SST

remains the same as the local equilibrium SST regardless of the processes in the Tropics. Effectively, the infinitely large midlatitude box provides an infinite cold water source for the upwelling water to the surface equator (as in MG and ND). Therefore, the box model essentially reduces to a two-box model for the surface equatorial ocean. For further simplicity, we also assume that all the upwelling water flows into the western equatorial box ($\epsilon = 0$) before leaking out to the extratropics. Thus, (2.7b) reduces to $B(Q) = (1 + Q)^2$. This two-box model will be called the simple two-box model. This is the model that will be studied in this section, unless otherwise specified.

a. The formation of WCWC

In the surface equatorial regions, for weaker Walker coupling, only the steady-state $Q = 0$ in (3.1a) is physically valid ($Q \geq 0$). It is also stable. Thus, we have a single stable state

$$T_1 - T_2 = 0 \text{ and } T_1 - T_3 = 1 \text{ for } A_w \leq 1, \tag{3.3}$$

or $T_1 = T_2 = 1$ (in dimensional form, $T_1^* = T_2^* = T_E$). This is the local equilibrium state with no zonal SST gradient, no ocean currents, and no Walker circulation. Thus, $A_w < 1$ will be called the local equilibrium regime (Figs. 2a,b).

For strong Walker coupling, however, the steady state (3.4) becomes unstable. Instead, a new stable steady state emerges from (3.1b) as

$$Q = \sqrt{A_w} - 1; \tag{3.4a}$$

$$T_1 - T_2 = (\sqrt{A_w} - 1)/A_w \text{ and}$$

$$T_1 - T_3 = (2\sqrt{A_w} - 1)/A_w \text{ for } A_w \geq 1. \tag{3.4b}$$

This state has a finite zonal SST gradient, ocean transport, and Walker circulation. With the increase of A_w , the SSTs decrease in both the warm pool and cold tongue (Fig. 2a). The west–east SST difference and the total transport are also plotted in Fig. 2b. The finite west–east SST difference corresponds to a finite Walker circulation surface wind. Thus, with $A_w > 1$, a finite WCWC will be established. For the Pacific, our early estimate of the coupling parameter $A_w \approx 4$ in the Pacific is strong enough to destabilize the local equilibrium and therefore to initiate the WCWC. The WCWC formation mechanism here agrees with that of ND. The local equilibrium state is destabilized (the symmetry breaking) by the Bjerknes wind–upwelling positive feedback. The destabilization can be realized by an increased coupling strength, as pointed out by ND, as well as an increased latitudinal differential heating or a weaker local air–sea thermal coupling, according to the dimensional form of A_w in Eq. (2.5d). In fact, an increase of the coupling strength increases the efficiency of the coupled system in generating ocean currents, an increase of the local relaxation time will make the ocean advection relatively

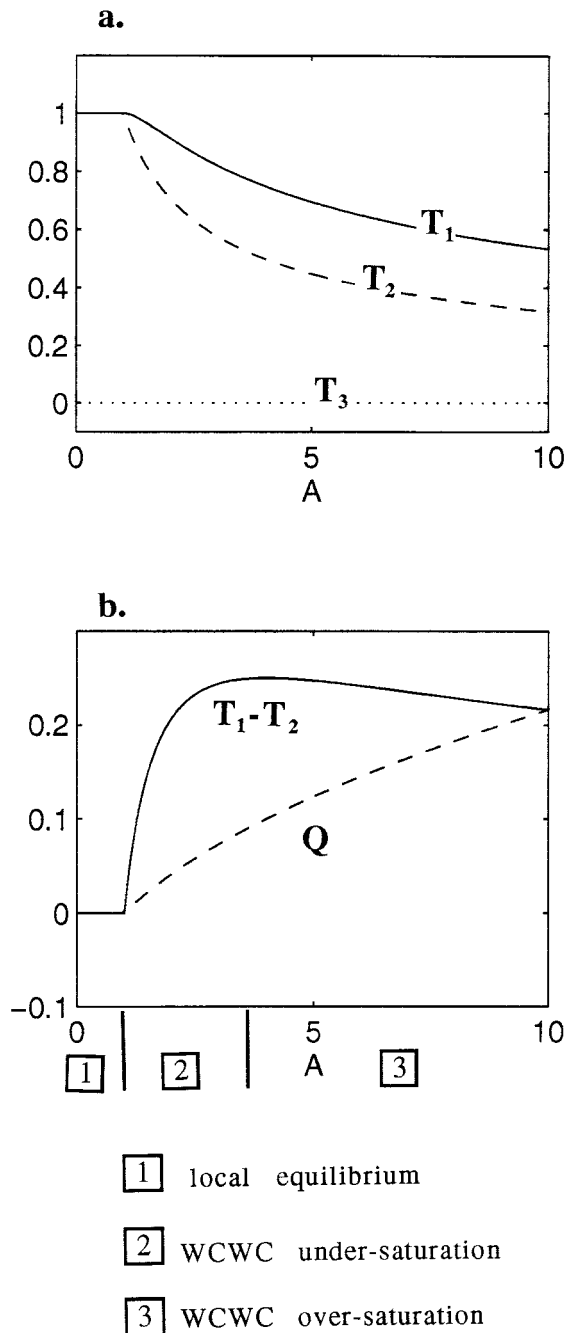


FIG. 2. The stable steady-state nondimensional solutions as functions of the Walker coupling parameter $A = A_w$ in a simple two-box model ($m = \infty$ and $\epsilon = 0$) without Hadley coupling ($A_H = 0$). (a) Temperatures in each box and (b) zonal SST difference and transport (latter multiplied by 0.1). Although the transport increases monotonically with the Walker coupling parameter A , the zonal SST difference exhibits different behaviors in three regimes: the *local equilibrium* regime ($A \leq 1$), in which no zonal SST difference exists; the *WCWC undersaturation* regime ($1 \leq A \leq 4$), in which the strength of west-east SST difference increases with the coupling parameter A ; and the *WCWC oversaturation* regime, in which the strength of the zonal SST difference decreases with the coupling parameter A .

more important compared with the surface forcing, and an increased latitudinal differential heating increases the external forcing to the coupled system. All three factors tend to intensify the ocean-atmosphere feedback and therefore the cold upwelling on the equator. This positive feedback increases the surface heat flux that eventually balances the cold upwelling to maintain the coupled WCWC system at a finite amplitude (appendix).

b. Regulation of WCWC

Here, we present the core material of the paper—the saturation of the WCWC system. First, we notice that the increase of A_w causes a monotonical increase in the oceanic transport Q [Eq. (3.5a) or Fig. 2b] and a monotonical decrease of the SSTs in both the eastern and western boxes (Fig. 2a), but not the zonal SST difference in Eq. (3.5b) (solid line in Fig. 2b)! Indeed, at the transport of $Q_m = 1$, $T_1 - T_2$ reaches its maximum, or saturation level, of

$$T_1 - T_2 \Big|_{\max} = 1/4 \quad \text{at} \quad A = A_{wm} \equiv 4, \quad (3.5a)$$

or in dimensional form,

$$T_1^* - T_2^* \Big|_{\max} = (T_E - T_M)/4. \quad (3.5b)$$

This upper bound is only one-quarter of the trivial upper bound $T_E - T_M$ of the coupled system! The saturation of zonal SST difference also implies a saturation for the Walker circulation. Thus, with an increased coupling, the intensity of the WCWC increases only for weak coupling for $A_w < A_{wm}$. With strong coupling for $A_w \geq A_{wm}$, the intensity of the WCWC starts to decrease, although the ocean transport continues to increase. Thus, the solution for $A_w > 1$ can be divided into two sub-regimes: the WCWC undersaturation regime for $1 < A_w < A_{wm}$ and the WCWC oversaturation regime for $A_w \geq A_{wm}$ (Fig. 2b).

For a given differential heating $T_E - T_M$ and a coupling strength A_w^* , one can further show that the warm pool surface heat flux reaches its maximum at the WCWC maximum state with a restoring time $\tau_{rm} = A_{wm} m_1/A_w^*(T_E - T_M)$ (the cold tongue surface heat flux achieves its maximum value at a shorter restoring time $3\tau_{rm}/4$). The surface heat flux decreases with either an increase or a decrease of the restoring time. Thus, the WCWC maximum state also represents the maximum flux state in the warm pool. Now, the ocean adjusts itself to stay in the most efficient state for absorbing the heat in the warm pool.

It is likely that the present climatology of the Pacific is in the vicinity of the saturation WCWC state. Equation (3.6b) shows that WCWC is regulated by an upper bound, which corresponds to an equatorial west-east SST difference about one-quarter of that of the latitudinal local equilibrium SSTs. In the Pacific, a reasonable estimate of the latitudinal difference of local equilibrium SST can be put at 20°C . This will put the upper bound for the zonal SST difference at about $4^\circ\text{--}5^\circ\text{C}$, agreeing

well with our present observation. This is also consistent with the estimate of $A_w \approx 4$ for the Pacific, which is close to the $A_{wm} = 4$ value.

The upper bound [Eq. (3.6)] may seem surprising at first sight. It is easy to understand that the zonal SST difference has to be limited by the trivial upper bound—the latitudinal differential equilibrium SSTs, or $T_1 - T_2 \leq T_E - T_M$. However, one may speculate that this trivial upper bound is achievable and, furthermore, that it would be reached in the limit of strong coupling. Our result shows that both speculations are wrong. The zonal SST difference has an upper bound that is only one-quarter of the trivial upper bound, and the upper bound is reached at a finite coupling strength.

This can be understood as follows. First, one should notice that the ocean current intensifies with the coupling monotonically, but not with the zonal SST gradient (or WCWC). If the current is so strong that the effect of local relaxation becomes negligible, the zonal SST field will become almost uniform downstream. In other words, the tendency of the Bjerknes positive feedback to generate a strong WCWC is offset by the tendency for a strong current, which generally produces a uniform downstream SST and therefore decouples the downstream SST gradient from the current strength. A saturation SST gradient (or WCWC) is then achieved when the timescale for the advection is comparable to that of the local equilibrium process. This is the case in our model because $Q_m = 1$.

The decoupling of SST gradient from strong ocean currents in the oversaturation regime also suggests that the regulation arises purely from the ocean dynamics of the coupled model, or independent of the dynamic coupling. To confirm this, an uncoupled ocean-alone model is used. The ocean-alone model is essentially the same as the coupled model in Eq. (2.4), except that the ocean current Q is regarded as a prescribed wind-driven current. For steady states, Eq. (2.8a) then gives

$$T_1 - T_2 = \frac{Q}{(1 + Q)^2}. \quad (3.6)$$

This relation (Fig. 3) shows clearly that the zonal SST difference increases with the transport only for weaker currents $Q < Q_m \equiv 1$ in the undersaturation regime. For stronger currents, the SST gradient starts to decrease. The maximum zonal SST gradient is achieved at $Q = 1$, when the advective time is comparable to the local relaxation time. For weaker currents in the undersaturation regime, the currents tend to build up the zonal SST difference, which is partially canceled by the local equilibrium process that restores the SST toward the zonally uniform equilibrium SST. However, for a stronger current in the oversaturation regime, the role of ocean advection is reversed to also generate a uniform downstream temperature. Thus, the regulation of maximum SST gradient (or WCWC) in the coupled model is caused by the kinematic tendency of the ocean itself

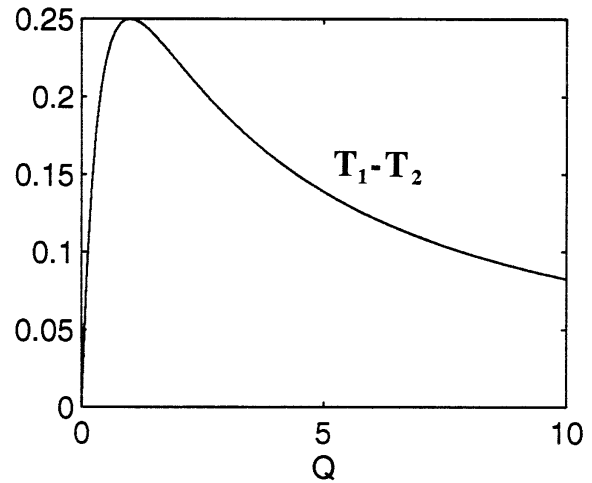


FIG. 3. The steady-state solution for the uncoupled ocean-alone two-box model with $m = \infty$ and $\epsilon = 0$. Nondimensional zonal SST difference is plotted as a function of transport Q . This is the same as plotting the zonal SST difference against the transport of the corresponding coupled case in Fig. 2b.

to decouple its zonal SST gradient from the strong wind drift current. This is reminiscent of some studies in the midlatitude ocean (Wang et al. 1995; Klinger 1996).

Although dynamic coupling is not essential for the WCWC regulation, the thermodynamic coupling through the local negative air–sea feedback is crucial. Indeed, if one uses a fixed equatorial heat flux $H_1 = H_2 = H_e$ [model (2.1), as in MG] instead of a restoring forcing [in Eq. (2.2)], one can derive the steady-state solution as $T_1 - T_2 \propto H_e/Q \propto \sqrt{H_e/A_w}$. Thus, the zonal SST difference is unbounded in the limit of weak coupling and decreases monotonically with coupling strength. Only the oversaturation regime exists.

c. General box model

The simple two-box model discussed above, although extremely simple, gives results that agree remarkably well with a general box model. Figure 4 plots the stable steady-state solution the same as in the simplest 2-box solution in Fig. 2, but for a more realistic parameter $m = 3$ and $\epsilon = 0.3$. All the features remain the same as in Fig. 2, but for a warmed up midlatitude T_3 (Fig. 5a), which is caused by the feedback of the poleward heat transport from the surface equatorial ocean on a finite midlatitude ocean. Further calculations show that the model solution is not very sensitive to the model parameters in the realistic regime, say $m > 1$ and $\epsilon < 0.5$ (not shown).

The insensitivity of the solution to model parameters can also be seen clearly for the saturation state of WCWC, as shown in Fig. 5, which plots the saturation SST difference, the corresponding coupling parameter A_{wm} , and transport Q_m as functions of m and ϵ . First of all, $T_1 - T_2 |_{\max}$, A_m and Q_m are insensitive to m , and

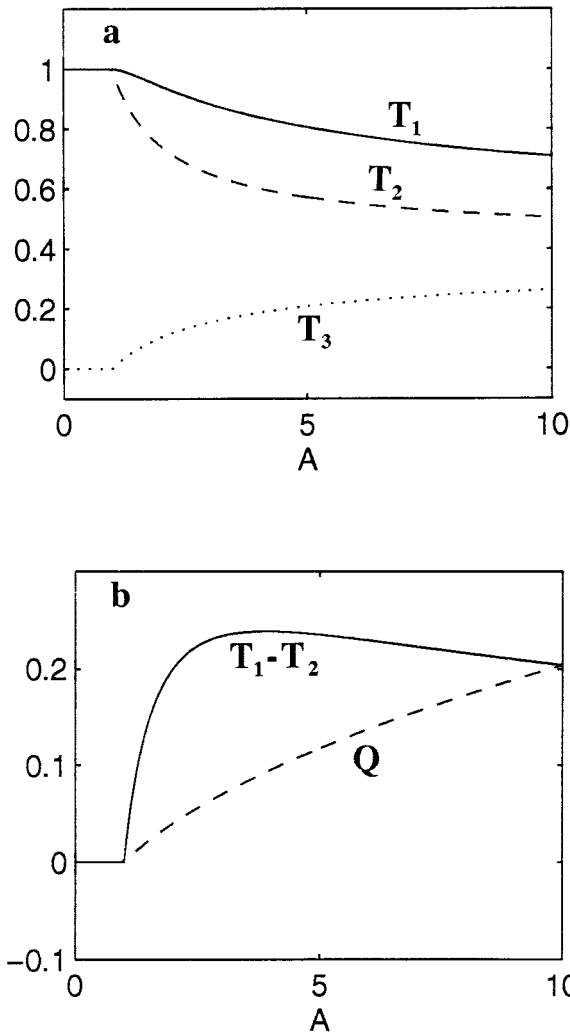


FIG. 4. Same as in Fig. 2 but for a more general box model with $m = 3$. The finite volume in box 3 allows the feedback of the heat transport from the equatorial boxes to warm the midlatitude box temperature T_3 . Otherwise, the solution qualitatively resembles the two-box model solution in Fig. 2.

ϵ in the realistic range of $m > 1$ and $\epsilon < 0.5$. For example, $T_1 - T_2 |_{\max}$ is between 0.2 and 0.3, A_m is between 2.5 and 5, and the transport Q_m is between 0.6 and 2. These are close to the values of 0.25, 4, and 1, respectively, in the simple two-box case in Eq. (3.6). This insensitivity is caused by the compensating effects between the decrease of m (from ∞) and the increase of ϵ (from 0). A decrease of m increases the warming response of the midlatitude ocean to the heat transport from the Tropics. This produces a warmer thermocline water and therefore reduces the upwelling cooling. The reduced cooling increases the SST more in the cold tongue than in the warm pool and, therefore, reduces the zonal SST difference. To the contrary, an increase of ϵ reduces the zonal advection of the cold water from the cold tongue into the warm pool. This intensifies the

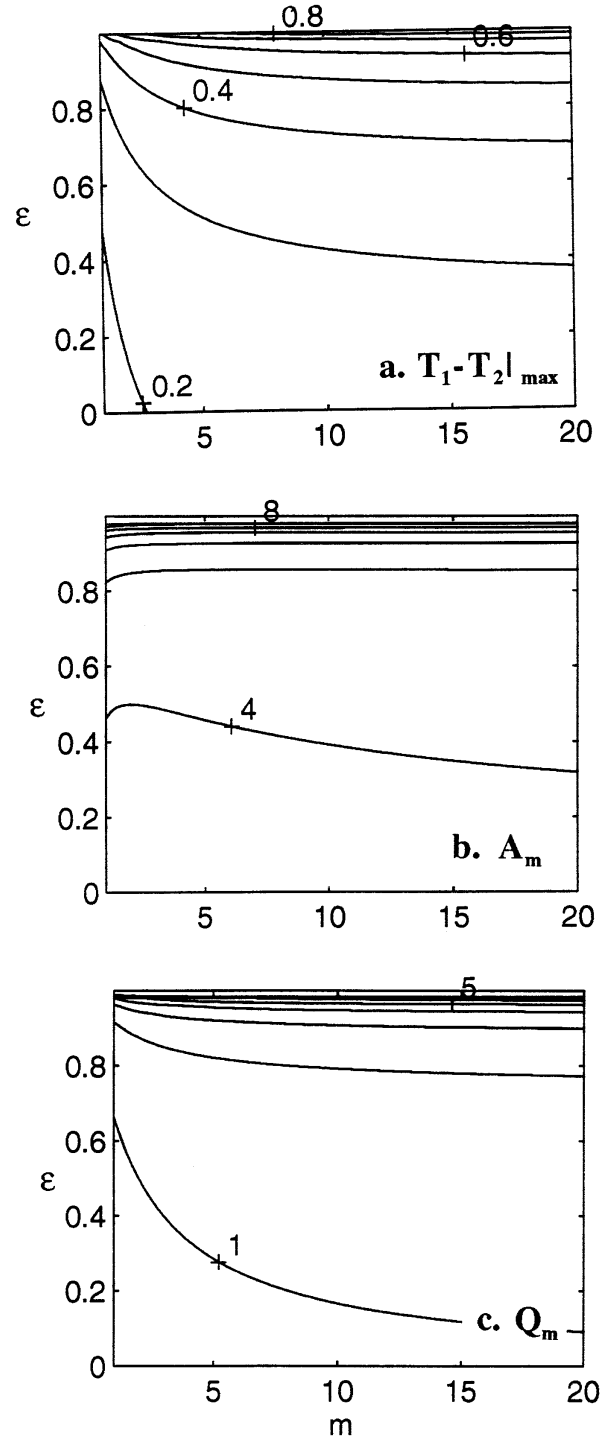


FIG. 5. Sensitivity of the maximum WCWC state to model parameters m and ϵ for the general box model (without Hadley coupling). (a) The maximum west-east SST difference (contour interval 0.1), (b) the corresponding coupling parameter (contour interval 1), and (c) the corresponding transport (contour interval 1). The sensitivity is very weak for the realistic regime of $m > 1$ and $\epsilon < 0.5$.

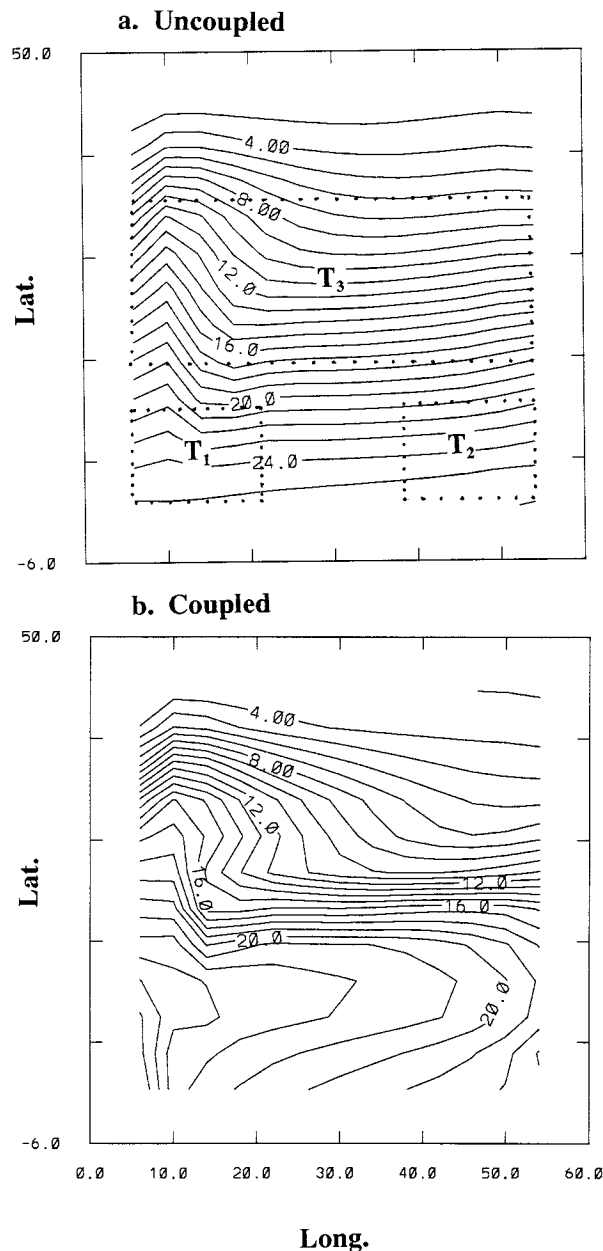


FIG. 6. SSTs for two GCM runs, which have a restoring time of 200 days and a restoring temperature profile with its maximum at 36°C at the equator (see later Fig. 13). (a) The steady state in the absence of wind forcing and (b) the steady state for the coupled run with the Walker coupling parameter $p = 0.325$.

warming in the warm pool and the cooling in the cold tongue. As a result, the zonal SST difference is increased.

Finally, in the extreme case of $\epsilon \rightarrow 1$ and $m \rightarrow \infty$, the saturation level approaches the true trivial limit 1. Now, opposite to the MG limit ($\tau_r \rightarrow \infty$), there is no oversaturation regime, while the coupled system is always in the undersaturation regime. This is the case of ND, which neglects the zonal advection along the equator

($\epsilon = 1$) and which assumes a fixed subsurface ocean temperature ($m \rightarrow \infty$). The neglect of the zonal advection leaves the warm pool always in the local equilibrium $T_1^* = T_E$. The cold tongue, on the other hand, can strongly interact with the extratropics and be cooled to $T_2^* = T_M$.

In short, the WCWC can be initiated by the wind-upwelling feedback. The strength of the WCWC is regulated by an upper bound due to the kinematic decoupling of SST gradient from strong ocean currents. Furthermore, the coupled dynamics of WCWC do not show significant sensitivity to model parameters in the realistic parameter range of $m > 1$ and $\epsilon < 0.5$. This suggests that the formation and regulation of the coupled WCWC system are robust features in more realistic models, such as general circulation models. This is confirmed in the following section.

4. Ocean general circulation model

As a further step, the Geophysical Fluid Dynamics Laboratory MOM model is used. Here, we use a model ocean that has a domain of $(0^\circ, 60^\circ) \times (6^\circ\text{S}, 50^\circ\text{N}) \times 3000$ m and a resolution of $4^\circ \times 4^\circ \times 15$ layer, with a surface layer of 20 m. The southern boundary at 6°S turns out to have no significant effect because experiments with a southern boundary at 50°S give similar results (see later Figs. 11 and 12). The lateral viscosity and dissipation coefficients are 10^9 and 10^7 $\text{cm}^2 \text{s}^{-1}$, respectively, and the vertical viscosity and dissipation coefficients are 10 and 1 $\text{cm}^2 \text{s}^{-1}$, respectively. Salinity is kept uniformly constant at 35 psu. Each run is spun up for 1000 surface yr (5000 bottom yr), forced only by a surface restoring temperature that can be thought of as the local equilibrium SST in the box model. This generates a strong thermohaline circulation—an important ocean circulation component that is absent in our box model. Various surface restoring time τ_r and latitudinal restoring temperature profiles $T_E(\theta)$ are used. In section 4b Fig. 8a shows the SST pattern at the end of one spinup run, with $\tau_r = 200$ days, and a $T_E(\theta)$ that has the maximum of 36°C on the equator (see later Fig. 13). Several features are noteworthy. First, little zonal SST gradient is generated on the equator, implying that a thermohaline alone contributes little to the zonal SST gradient on the equator. Second, the latitudinal SST gradient is much smaller than that of the restoring temperature (also in Fig. 13) because of the poleward heat transport of the thermohaline circulation. Therefore, unlike in the box model, the SST after spinup is not the same as the local equilibrium SST (the restoring temperature), even in the absence of wind.

In order to study the coupled WCWC system, a hybrid coupled model is constructed by coupling MOM with a simple atmospheric zonal wind model. The zonal wind stress has a fixed latitudinal profile $P(\theta)$, which consists of easterlies in the Tropics (0.5 dyn cm^{-2} on the equator)

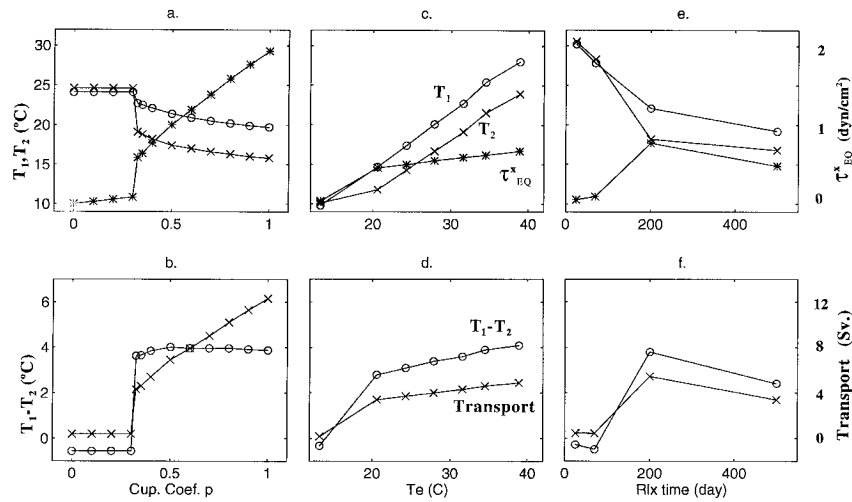


FIG. 7. Three sets of hybrid coupled GCM experiments for the warm pool and cold tongue SSTs ($^{\circ}\text{C}$) and the wind stress on the equator (dyn cm^{-2}) (a), (c), and (e); and the warm pool–cold tongue SST difference ($^{\circ}\text{C}$) and transport (Sv) (b), (d), and (f) in the absence of Hadley coupling. (a) and (b) For 12 runs that have the same restoring temperature and time as those in Fig. 6, but have a different Walker coupling parameter p . The model blows up for $p > 1$. Extra experiments (not shown) show that the transition value between the local equilibrium regime and WCWC onset regime occurs sharply at $p = 0.318$. (c) and (d) For six runs with a restoring time of 200 days and a coupling coefficient of $p = 0.325$, but with different restoring temperature profiles (see Fig. 13). (e) and (f) For four runs with the same restoring temperature as in Fig. 6 and a coupling coefficient of $p = 0.4$, but with four different restoring times.

and westerlies in the midlatitudes. The magnitude of the wind stress is coupled to the zonal SST difference as

$$\tau^x = p(T_1 - T_2)P(\theta) \Lambda(T_1 - T_2), \quad (4.1)$$

where p is part of the total Walker coupling parameter A_w^* in Eq. (2.3a). We also use T_1 and T_2 , respectively, to simulate the SSTs of the western and eastern surface equatorial boxes in the four-box ocean. The T_1 and T_2 are calculated as the spatially averaged SST over the western and eastern one-third of the basin and within 10° of the equatorial belt (indicated in Fig. 6a). The sign function is $\Lambda(\eta) = 1$ for $\eta \geq 0$ and $\Lambda(\eta) = 0$ for $\eta < 0$, where η is any variable, such that we only keep the easterly wind on the equator. The initial state for each coupled run is the final thermohaline spunup state, perturbed by the addition of a small, cold SST anomaly in the eastern equator. A quasi-equilibrium coupled solution is reached in several decades, and results shown below are at the end of year 100.

a. Formation of WCWC

The GCM solutions also exhibit three regimes as in the box model. We start with the local equilibrium regime and the WCWC undersaturation regime. Figures 7a,b present 12 coupled experiments, which are the same as those run in Fig. 6a, except for a different coupling parameter p . For weak coupling $p < 0.3$, the solution remains the same as the steady state (Fig. 7a), with little zonal SST difference, upwelling transport (Fig. 7b), or surface wind stress (in Fig. 7a). As noted before, this

state is in the thermohaline equilibrium, rather than the real local equilibrium that has neither ocean current nor mixing. Nevertheless, for convenience, it will still be called the local equilibrium state.

For strong coupling at about $p = 0.32$, the solution changes dramatically. The SST is cooled by 6°C in the cold tongue and 2°C in the warm pool (Fig. 7a). The cooling is accompanied by a jump of 4°C in the zonal SST difference, of 5 Sv in the upward transport into the cold tongue (Fig. 7b), and of 0.5 dyn cm^{-2} in the equatorial easterly wind stress (Fig. 7b). One example of the SST field is shown in Fig. 6b for $p = 0.325$. Thus, the GCM confirms the transition between the local equilibrium regime to the WCWC undersaturation regime.

The transition to the undersaturation regime should also occur if either the latitudinal differential heating $T_E - T_M$ or the local restoring time τ_r is increased. This is because the onset is determined by the increase of the nondimensional coupling parameter $A_w = \tau_r a(T_E - T_M)/m_1$, as shown in the box model [see Eqs. (2.5d)]. Hence, two additional sets of coupled experiments are carried out. Figures 7c,d show 7 runs, which are the same as those in Fig. 6b, except for different restoring temperature profiles (see Fig. 13). For the weak differential heating case of $T_E < 20^{\circ}\text{C}$ (where T_E is defined as the restoring temperature averaged within a 10° latitude belt), the tropical SSTs are almost identical between the east and west (Figs. 7c,d), and there exists little upwelling transport (Fig. 7d) or wind stress (Fig. 7c). This is the local equilibrium regime. When T_E exceeds 20°C , a further increase in restoring temperature

results in a dramatic cooling in the cold tongue, yet a rather weak warming in the warm pool (Fig. 7c). The zonal SST difference, upwelling transport (Fig. 7d), and surface wind stress (Fig. 7c) increase dramatically, indicating the onset of a WCWC.

Figures 7e,f further test the effect of various restoring times. The four runs shown are the same as those in Fig. 6b, except for $p = 0.4$ and with different restoring times. For short restoring times of 20 days and 75 days, the system returns to the local equilibrium state (Figs. 7e,f). When the restoring time reaches 200 days, a finite WCWC emerges, with a finite zonal SST difference (Figs. 7e,f), wind stress (Fig. 7e), and ocean transport (Fig. 7f). This is the WCWC undersaturation regime.

Hence, the GCM experiments confirm that the transition from the local equilibrium regime toward the WCWC undersaturation regime occurs with the increase of the coupling strength, the latitudinal differential heating, or the restoring time.

b. Regulation of WCWC

We further discuss the oversaturation regime of the coupled model solution. For coupling much stronger than the transition value $p = 0.32$, the equatorial SSTs are cooled further (Fig. 7a), while the upwelling transport (Fig. 7b) and wind stress (Fig. 7a) are increased further. In contrast, the zonal SST difference (Fig. 7b) increases slightly and then starts to decrease after $p > 0.5$. This confirms the transition from the undersaturation regime to the oversaturation regime.

After the onset of WCWC (with T_E larger than 20°C) and with the increase of the latitudinal differential heating, the equatorial SSTs and the upwelling transport increase further, as does the zonal SST difference. To check the consistency of the solution with the saturation level in Eq. (3.6a), the normalized zonal SST difference is also calculated as $(T_1 - T_2)/(T_E - T_M)$. For sensitivity purposes, several choices of the midlatitude surface T_M are used. This ratio is found to be around 0.2 (not shown), agreeing well with the 0.25 upper bound in the box model.

With the increase of the restoring time, Figs. 7e,f show a somewhat different picture. When the restoring time increases from 200 days to 450 days, the cold tongue SST remains almost unchanged and the warm pool temperature decreases only slightly (Fig. 7e), resulting in a decrease of the zonal SST difference (Fig. 7f). This seems to resemble the transition from the undersaturation to the oversaturation regime. However, unlike the two previous sets in Figs. 7a,b and Figs. 7c,d, the upwelling transport also decreases (Fig. 7f). This is opposite to the box model result. Therefore, this transition is caused, at least partly, by mechanisms that are absent in the box model. The thermohaline circulation seems to be a candidate.

As in the box model, uncoupled ocean-alone experiments are carried out to confirm the role of ocean cir-

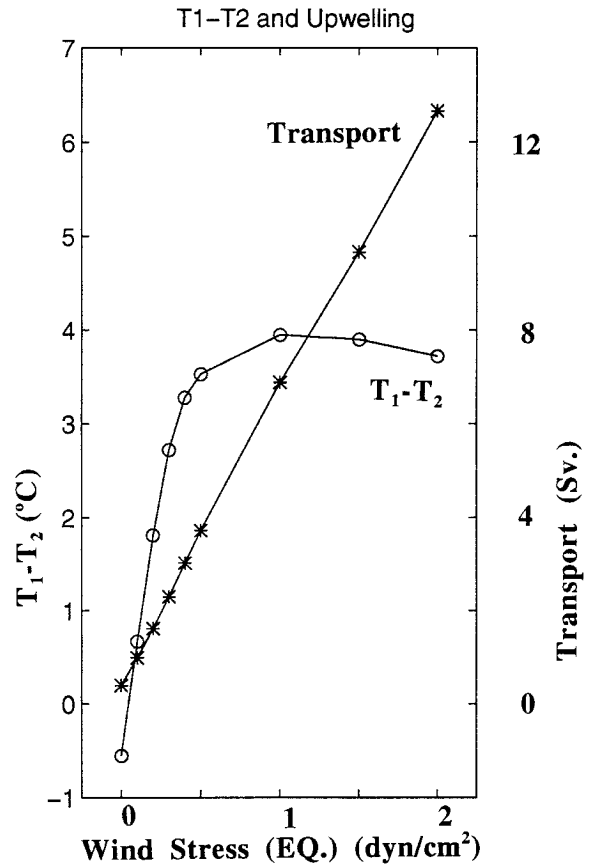


FIG. 8. The uncoupled ocean-alone model experiment. Nine runs are shown, with the zonal SST difference (circled curve, in $^\circ\text{C}$) and net upward transport [star curve, in Sv] ($1 \text{ Sv} = 10^6 \text{ m s}^{-1}$) plotted against the magnitude of the wind stress on the equator (dyn cm^{-2}). If plotted with the SST difference against the transport, the figure will resemble the box model solution in Fig. 3. The most salient feature is the monotonical increase of the transport with the wind stress, but a initial increase and a later slight decrease of zonal SST difference, indicating the saturation of the WCWC and the decoupling of SST gradient from the ocean transport.

ulation in the regulation of WCWC. Figure 8 plots nine experiments, which are the same as those in Figs. 6a,b, except for prescribed wind forcings. As the wind stress increases, the upwelling transport increases almost linearly. In contrast, the zonal SST difference levels off at about 4°C when the equatorial wind reaches about 1 dyn cm^{-2} , both values being consistent with those in the corresponding coupled run in Figs. 7a,b. The plot with the SST difference against the transport (not shown) has a curve pattern similar to that of the SST difference curve in Fig. 8 and, therefore, is similar to the box model ocean-alone case in Fig. 3.

The GCM results are not sensitive to the wind pattern. Identical experiments are carried out, except with a uniform easterly wind pattern in the entire domain (not shown). No qualitative differences are found. Experiments have also been carried out for a doubled resolution that has a smaller viscosity. No substantial dif-

ference is found, except that the initialization and saturation of the WCWC are realized for a weaker Walker coupling parameter p [or a_3 in Eq. (2.3a)]. This is obvious because the small viscosity effectively increases the wind-driven current [or a_1 in Eq. (2.3a)].

5. Interaction with the Hadley circulation

We now extend the study to include the Hadley coupling effect, such that the wind and, in turn, the current depend on not only the zonal SST gradient but also the meridional SST gradient [as in Eq. (2.3) or (2.5)]. For simplicity, we limit ourselves to the simple two-box model case ($m = \infty$, $\epsilon = 0$), while the general box model gives similar results.

a. Hadley coupling and WCWC regulation

The Hadley circulation can force tropical easterlies in the absence of the Walker circulation. Therefore, it is conceivable that the inclusion of Hadley coupling can force a WCWC even in the absence of Walker coupling. One can show from the solution for Eqs. (2.7) and (2.8) that an infinitesimal Hadley coupling parameter $A_H > 0$ can initialize a WCWC. Therefore, as far as the establishment of the WCWC is concerned, the Walker coupling, or the Bjerknes positive feedback, is not crucial in the Pacific, where the meridional SST gradient seems to be able to force a Hadley circulation. The Walker coupling, however, can reinforce the Hadley coupling. In other words, an increase of A_H is dynamically equivalent to an increase in A_w ; it would monotonically increase the transport, and decrease the SSTs and the meridional SST gradient.

The Hadley coupling, just like the Walker coupling, does not affect the saturation level of the WCWC. This is easy to understand because the saturation of WCWC is determined by the kinematic advection effect of the ocean current, as discussed before. Indeed, the saturation level can be derived directly from the solution for Eq. (2.8a) at an optimal transport $Q_m = 1$ ($m = \infty$, $\epsilon = 0$), which is dependent on neither A_H nor A_w . However, since the Hadley coupling and Walker coupling reinforce each other, one should expect the saturation to be achieved at $A_w < 4$ when $A_H > 0$. The discussion above can be seen in Fig. 9, which plots the zonal SST difference as a function of A_w for several A_H values. The existence of the Hadley coupling produces a nonzero SST difference even in the absence of Walker coupling ($A_w = 0$). The Walker coupling parameter that is required to reach the saturation decreases with the increase of A_H . This can be seen explicitly by inserting $Q = Q_m = 1$ into the transport equations (2.7a) and (2.7b). In the simple two-box case, this gives $2A_w + 5A_H = 8$. Thus, the saturation A_w is bounded by $A_w = 4 - 5A_H/2 \leq 4$, while the saturation Hadley coupling parameter is bounded by $A_H = 8/5 - A_w/4 \leq 8/5$. For $A_H > 8/5$, the

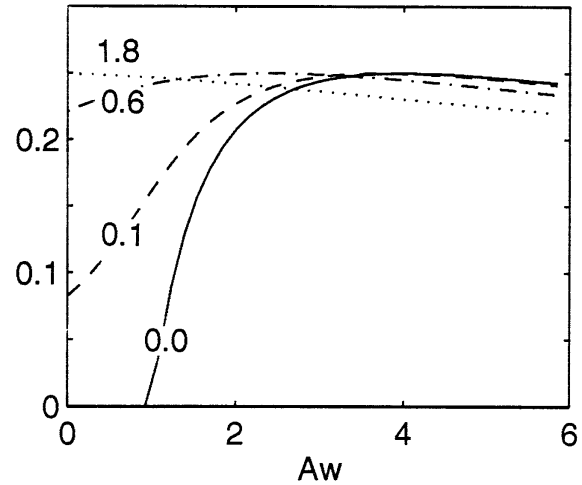


FIG. 9. Nondimensional solutions of zonal SST difference for the simple two-box model stable steady state as functions of the Walker coupling parameter A_w in the presence of Hadley coupling of $A_H = 0.0, 0.1, 0.6$, and 1.8 . It is seen that the Hadley coupling enhances the Walker coupling effect, but does not change the saturation level of the zonal SST difference.

WCWC always lies in the oversaturation regime, as does the curve of $A_H = 1.8$ in Fig. 9 (dotted line).

b. Relative efficiency of Hadley and Walker coupling

The discussion above suggests a dynamic similarity between the Hadley and Walker coupling. Both can (i) initiate the WCWC, (ii) intensify the transport, (iii) regulate the WCWC, and (iv) reduce the meridional SST gradient. The next question is then, which coupling is more efficient? This can be estimated in the following way. The efficiency of the Hadley and Walker coupling can be measured by $\partial Q/\partial A_H$ and $\partial Q/\partial A_w$, respectively. From Eqs. (2.5a) and (2.5b), one can derive $\partial Q/\partial A_H/\partial Q/\partial A_w$ to be identical to $(T_{EQ} - T_3)/(T_1 - T_2)$. Equation (2.8) then gives the relative efficiency (at $\epsilon = 0$) as

$$\begin{aligned} (\partial Q/\partial A_H)/(\partial Q/\partial A_w) &\equiv (T_{EQ} - T_3)/(T_1 - T_2) \\ &= 3/2 + 1/Q \geq 3/2. \end{aligned} \quad (5.1)$$

Thus, the Hadley coupling is always more efficient than the Walker coupling. Furthermore, Eq. (5.1) suggests that in the limit of strong coupling (thus, $Q \rightarrow \infty$), the relative efficiency approaches a constant value $3/2$. This can be seen in Fig. 10, which shows the transport and zonal SST difference in the A_H and A_w parameter plane. The slope of the constant Q contour in Fig. 10a approaches the $3/2$ once A_H and A_w become modestly strong. Correspondingly, the slope of a constant zonal SST difference contour also approaches constant because the solution is determined by Q , as shown in Eq. (2.8). Furthermore, the saturation is seen to be achieved in a wide range of coupling parameters in Fig. 10b, although the transport increases monotonically with either A_H or A_w in Fig. 10a.

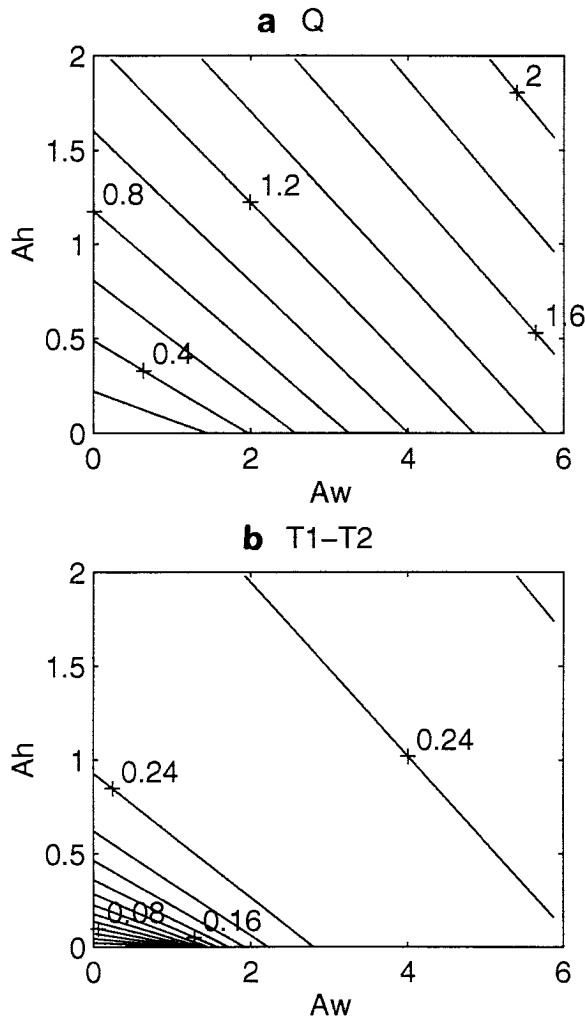


FIG. 10. Simple two-box model solutions as functions of the Hadley and Walker coupling parameters. (a) Transport and (b) zonal SST difference. At strong coupling limit, the solution is a function of a linear combination of A_w and A_h .

The relative efficiency is also related to the relative strength of the Hadley and Walker circulation. Noticing Eq. (5.1), we have $Q_H/Q_W \equiv A_H(T_{EQ} - T_3)/A_W(T_1 - T_2) = (3/2 + 1/Q)A_H/A_W \geq 3A_H/2A_W$. This of course depends on the unknown relative strength between the Hadley and Walker parameters. Yet, if we assume that the two coupling parameters are of comparable strength (not a very unreasonable assumption), we will have $Q_H/Q_W = 3/2$. Thus, the Hadley circulation is about 1.5 times stronger than the Walker circulation in the strong coupling limit.

c. GCM experiments

Hybrid coupled GCMs similar to those in section 4 are carried to confirm the box model solution. Now, the wind forcing depends on both the zonal and meridional SST gradients, as

$$\tau^x = [p_w(T_1 - T_2) + p_h(T_{EQ} - T_3)] \times \Lambda [p_w(T_1 - T_2) + p_h(T_{EQ} - T_3)] P(\theta). \quad (5.2)$$

Here, T_1 and T_2 are the SSTs averaged in the western and eastern halves within 10° of the equatorial belt, $T_{EQ} = 0.5(T_1 + T_2)$, and T_3 is the SST averaged within the latitudinal belt of ($12^\circ N, 38^\circ N$).

Figure 11 plots about 100 GCM solutions as a function of the Walker and Hadley coupling parameters p_w and p_h . Both the total wind (Fig. 11a) and the zonal SST difference (Fig. 11b) show remarkable resemblance to the corresponding box model variables in Figs. 10a,b. First, the total wind and zonal SST difference increases with a linear combination of p_w and p_h once the coupling is modestly strong. Furthermore, the efficiency for the Hadley coupling is stronger than that for the Walker coupling, which can be judged by the slower dependency with p_h than with p_w . Indeed, there is even a strong quantitative agreement with the box model results. The relative efficiency in Fig. 11 is now about $7/5$, slightly smaller than the $3/2$ in Fig. 10 [or Eq. (5.1)] (but the same as the box model result that uses $\epsilon = 0.2$). The other example is the relative contribution of the Hadley and Walker circulations to the total wind. This ratio is about 2 to 1 for $p_h \approx p_w$ in both the simple two-box model and the GCM (not shown).

In short, the Hadley coupling is dynamically similar to the Walker coupling. Both can establish the WCWC and regulate the WCWC. Quantitatively, the Hadley coupling is more efficient than the Walker coupling.

6. Atlantic WCWC

The Atlantic WCWC resembles that in the Pacific in many respects. However, it is considerably weaker than its counterpart in the Pacific because the SST difference in the Atlantic is less than one-third of that in the Pacific. One may speculate that the smaller size of the Atlantic is responsible for the difference. However, our theory [e.g., Eq. (3.6)] shows that the saturation level is independent of the basin size. Furthermore, the nondimensional coupling parameters in Eqs. (2.5c) and (2.5d) show that a smaller basin gives a faster advective time-scale and therefore enables the WCWC to reach saturation at a smaller (dimensional) coupling strength. All of these have been confirmed in our hybrid coupled GCM experiments with different basin sizes (not shown). The question is then, why does the one-quarter saturation level in Eq. (3.6) not apply to the Atlantic?

The reason is the zonal distribution of the trade wind, which in turn is caused by the adjacent land effect over the smaller Atlantic. The observed Pacific trade wind reaches its maximum in the middle ocean and therefore is symmetric between the eastern and western oceans. In contrast, the trade wind in the tropical Atlantic reaches its maximum in the west and its minimum in the east (not shown). This western-heavy wind profile is caused by the adjacent land effect. The stronger (weaker) east-

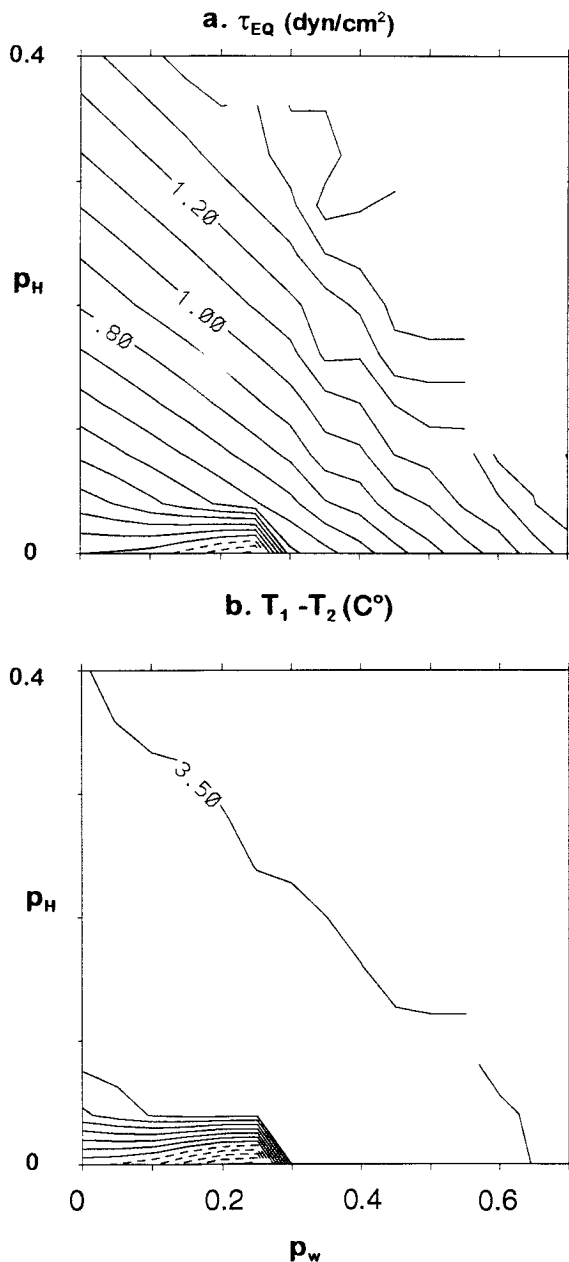


FIG. 11. Hybrid coupled GCM solutions (about 100 experiments) as functions of the Hadley and Walker coupling parameters. (a) Total wind stress on the equator (dyn cm^{-2} , contour interval 0.1) and (b) zonal SST difference ($^{\circ}\text{C}$, contour interval 0.5). The solutions compare well with the box model solution in Fig. 10. The experiments are calculated for each pair of the p_w and p_H , where p_w takes the 11 values 0.0, 0.05, 0.1, 0.15, 0.2, 0.25, 0.3, 0.4, 0.5, 0.6, and 0.7; and p_H takes 8 values 0.0, 0.01, 0.025, 0.05, 0.1, 0.2, 0.3, and 0.4. The results are then plotted on the regular p_w and p_H grid after interpolation. Notice that the results are not plotted for very strong coupling where the model blows up. The model setting is similar to that in Fig. 6, but with a southern boundary at 50°S and a restoring time of 100 days.

erly in the west (east) is caused by the westward (eastward) surface wind that converges toward the deep convection region over the Brazilian (West African) continent. Furthermore, the narrow size of the Atlantic plays a critical, yet indirect, role by allowing the land effect to extend well into the entire Atlantic and therefore to change the wind profile to a western-heavy wind.

It is straightforward that the zonal distribution of trades can affect the zonal SST difference and, in turn, the saturation level of WCWC. For an eastern-heavy easterly wind, most of the upwelling should occur in the eastern basin. This is the case in the Pacific. Therefore, the theoretical saturation level in Eq. (3.5) applies because it assumes all the upwelling of water occurs in the eastern basin (see Fig. 1). However, under a western-heavy easterly wind forcing, the resulting upwelling should increase in the west to compensate the stronger divergent Ekman flow there (relative to the case with a uniform easterly wind). As a result, the zonal SST difference should decrease.

The effect of upwelling into the western basin can be studied by modifying the box model [Eq. (2.1) or Fig. 1] to allow part of the upwelling water to enter the western equator. One can then show that the zonal SST saturation level is reduced with the increase of the upwelling water into the western equator. Especially when the amounts of upwelling are equal between the west and east, there will be no zonal SST gradient.

The reduction of the zonal SST gradient for a western-heavy wind profile can also be seen in our OGCM (and hybrid GCM, not shown) experiments. Figure 12a shows the zonal SST difference for three sets of OGCM experiments that have different wind profiles (Fig. 12b). The wind stress is similar to that used in Fig. 8, but varies in the zonal direction from a uniform wind to a very western-heavy wind:

$$\tau^x = P(\theta), \quad (6.1a)$$

$$\tau^x = P(\theta)(1 - x/2L), \quad (6.1b)$$

and

$$\tau^x = P(\theta)(1 - x/L), \quad (6.1c)$$

where L is the width of the basin. Figure 12a shows clearly that the saturation zonal SST difference is reduced for an increasingly western-heavy wind. Furthermore, the zonal profiles of wind, net upwelling, and SST along the equator are plotted in Figs. 12b–d for three cases of different wind profiles. One sees clearly that the increase in the western-heavy wind profile increases the upwelling into the western equator (Fig. 12c) and reduces the zonal SST gradient (Fig. 12d) in the interior ocean.

7. Summary and discussions

A coupled theory is proposed to account for the intensity of the coupled warm pool, cold tongue, and

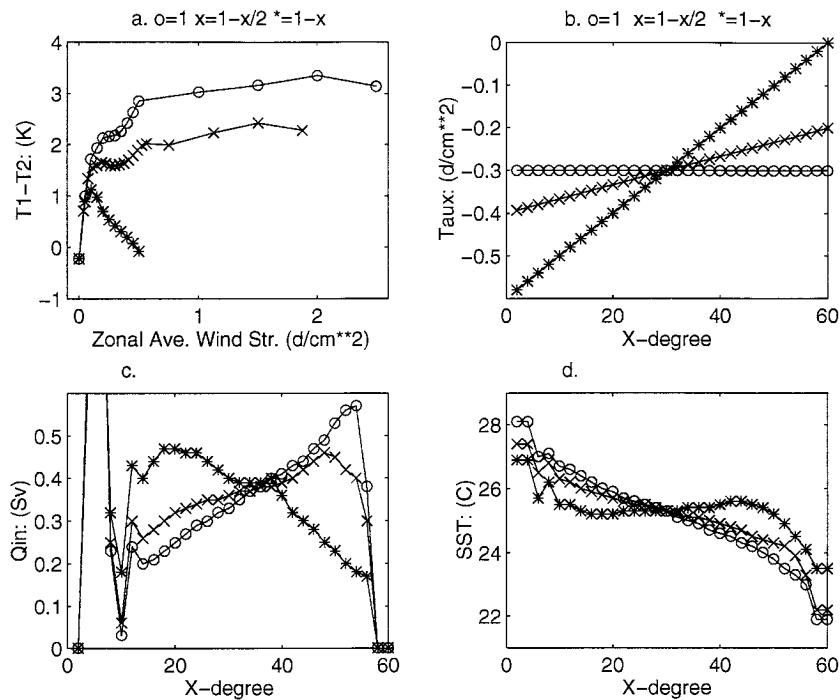


FIG. 12. Uncoupled ocean-alone GCM experiments for three sets of experiments with different wind profiles in Eqs. (6.1a) (circled curve), (6.1b) (crossed curve), and (6.1c) (asterisk curve). (a) The zonal SST difference between T_1 and T_2 , which are averaged in the western and eastern halves of the basin within 10° of the equator, respectively. The abscissa is the magnitude of the zonally averaged wind stress on the equator for each run. (b) The zonal distribution of the wind stress on the equator for the three runs in (a) that have the averaged wind magnitude of 0.3 dyn cm^{-2} . (c) The zonal distribution of the total incoming transport into the equatorial box that is bounded by 10° in latitude and 100 m in the depth [Sv (200 km^{-1})]. (The profile of total upwelling transport is similar; not shown.) (d) The zonal distribution of tropical SSTs that is averaged within 10° of the equator. The model setting is similar to that in Fig. 11, but with a resolution of $2^\circ \times 2^\circ \times 15$ level.

Walker circulation system in the Pacific. It is shown that the intensity of the WCWC is determined by the coupling strength, the local relaxation time, and latitudinal differential heating. Most importantly, it is found that, due to the ocean dynamics, the WCWC system is regulated much below the trivial upper bound—the latitudinal difference of equilibrium SSTs. The maximum zonal SST difference (and the associated Walker circulation) is only one-quarter of the latitudinal difference of equilibrium SSTs. Furthermore, the Hadley coupling acts dynamically the same way as the Walker coupling—both can initiate as well as regulate the WCWC. Finally, the much weaker WCWC in the Atlantic is caused by the western-heavy wind profile, which in turn is caused by the adjacent land effect that is able to extend deeply into the narrow Atlantic. In the following, we further discuss the implications and problems of the theory.

a. Tropical climatology

We believe that the consistent zonal SST gradient in the fully coupled GCM experiments of Mechoso et al.

(1995) can be interpreted as independent evidence of the saturation of the Pacific WCWC. Our theory can also be used to understand climate changes. The CLIMATE (Climate Long-Range Investigations, Mapping, and Prediction) SST seems to suggest an enhanced zonal SST difference. The simulated future climate with increased CO_2 shows a significant reduction of the Walker circulation in models with (Knutson and Manabe 1995) and without (Meehl and Washington 1996) flux corrections. The reason for the different changes of WCWC seems complex. In the global warming case, Knutson and Manabe (1995) argue that the evaporation in the warmer SST in the west tries to cool the SST more than it does to the east because the evaporation increases with increasing temperature due to the Clausius–Clapeyron dependence. Meehl and Washington (1996), on the other hand, find that the cloud–albedo feedback is important for the reduced SST gradient. Our theory may give another alternative. The CO_2 warming has a polar amplification, with the midlatitudes warmed more than the equator. This decreases the latitudinal differential equilibrium temperature and, in turn, the saturation level

of the WCWC according to Eq. (3.6b).² This view at least is consistent with both coupled experiments in that both find the oceanic advection that is sustaining the zonal SST gradient is reduced after global warming. In the case of the LGM climate, it is the opposite.

b. Climate variability

Recent years have seen intensive studies on ENSO (e.g., MG; Philander 1990; Neelin et al. 1994). Little attention has been paid to the relation between ENSO and the mean climatology. However, the interannual variability is very sensitive to the mean climatology. For example, in a coarse resolution global coupled model, a slight change of the mean climatology can change the direction of the propagation of the interannual variability from westward to eastward (Moore 1995). As another example, in a fine-resolution coupled GCM, the increase of the wind coupling by 10% completely eliminates the interannual variability (Latif et al. 1993). Indeed, as discussed by Neelin et al. (1994), the ENSO variability may be the first bifurcation of the tropical climatology with the increased coupling.

c. Regulation of tropical SST

One direct application of our theory is the regulation of the warm pool SST (Sun and Liu 1996). Recent studies on the regulation of tropical SST have focused on atmospheric processes (Newell 1979; Ramanathan and Collins 1991; Fu et al. 1992; Wallace 1992; Hartmann and Michelsen 1993; Pierrehumbert 1995). Our results show that the ocean dynamics may also play a significant role. Dynamic coupling can regulate the tropical SST by pumping cold water into the surface equator. Furthermore, since the west–east SST difference is regulated, the warm pool SST is closely tied to the cold tongue SST by surface wind drift currents. Therefore, the ocean current can regulate SST not only in the cold tongue, but also in the warm pool. For realistic parameters in the general box model, we can have dT_1^*/dT_E at about 0.7 and dT_2^*/dT_E even smaller. The regulation of tropical SST can also be seen in the GCM experiments in Fig. 7c. For the six runs in the WCWC regimes, one can estimate that $dT_1^*/dT_E = 0.78$ and $dT_2^*/dT_E = 0.66$. This is a strong regulation on the tropical SST, not only in the cold tongue, but also the warm pool.

To further examine the role of ocean–atmosphere coupling on the regulation of tropical SST, we plot in Fig.

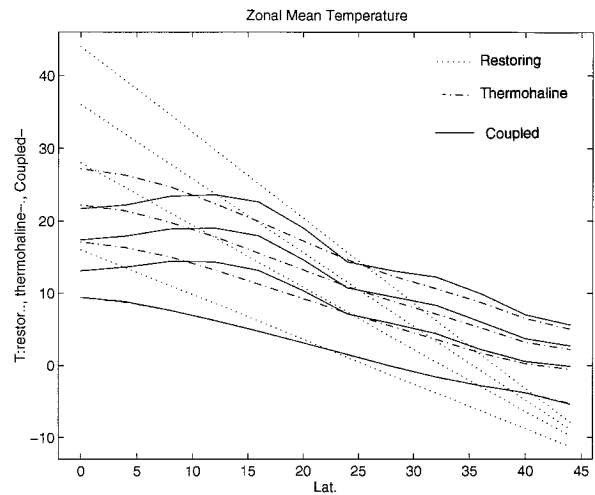


FIG. 13. Four restoring temperature profiles (dotted) (out of the seven used in Figs. 7c,d) and the corresponding zonal mean SST for uncoupled thermohaline-alone runs (dash-dotted), and coupled runs. Both the thermohaline-alone and the coupled WCWC (the upper three curves) reduce the tropical SST significantly. The coldest run is in the local equilibrium regime, and it therefore has the coupled solution overlapped with the thermohaline solution. This figure shows that the zonal mean tropical SST can be regulated significantly by both the buoyancy-driven thermohaline and the wind-driven thermocline processes. The model setting is the same as in Fig. 6.

13 the latitudinal profiles of the zonal mean SST and the restoring temperatures (dotted lines) for the 4 runs (out of the seven runs in Figs. 7c,d). Without winds, the SST has a much smaller latitudinal gradient than the restoring temperature. The SST can be colder than the restoring temperature by about 10°C in the Tropics, while the SST in the high latitudes can be warmer by 10°C. This means that the poleward heat transport of the thermohaline circulation alone can exert a strong regulation on the tropical SST, presumably on a long timescale. With the dynamic coupling, the tropical SST is further regulated significantly by the wind-driven heat transport. Different from the thermohaline, however, the effect of WCWC wind is mainly limited in the Tropics, where the SST can be lowered by more than 5°C. All of this indicates that one should be cautious with results of the warm pool SST regulation that are derived purely from local heat budget (Ramanathan and Collins 1991). This is consistent with some recent studies that call attention to the ocean dynamics in the regulation of tropical SST (Waliser 1996; Clement et al. 1996; Seager and Murtugudde 1997).

d. Problems

Our study has left many questions open. Although the box model agrees surprisingly well with the GCM, there are two differences in the strong coupling limit. First, the hybrid GCM starts to produce self-sustained oscillation at interannual to decadal timescales, while the box model never oscillates. Secondly, the zonal SST

² Recent studies of Clement et al. (1996) and Seager and Murtugudde (1996) have arrived at the opposite conclusion for the global warming case—that is, an increased zonal SST gradient under a uniform global warming. Our preliminary results show that this is related to the transient behavior of the system. While in the early stage the WCWC intensifies; the final equilibrium at multidecadal to century timescales will still approach our solution. This work will be reported elsewhere.

difference $T_1 - T_2$ shows a clear decrease for strong coupling in the box model (oversaturation regime), but not in the GCM. The reasons remain to be studied. The absence of wave process in the box model may be responsible for the absence of oscillation. To simulate the realistic ocean, the poor resolution and idealized nature of the OGCM experiments need to be improved. The strong viscosity undoubtedly suppresses the equatorial ocean currents and, in turn, the coupling and regulation.

Even more serious is the atmospheric model. The fixed wind pattern is rather unrealistic and remains to be improved with a more realistic wind model. An explicit inclusion of the atmospheric feedback may play an important role. It is likely that the atmospheric feedback can further regulate the WCWC system. For example, the Walker circulation can transport warm air from the western Pacific to the eastern Pacific, where the clear and dry atmosphere allows the heat to be radiated away efficiently. This effect further suppresses the west-east asymmetry and therefore regulates the WCWC.

The land effect and the related monsoon effect have not been considered. Our model applies best to the original Walker circulation over the Pacific equator, where ocean-atmosphere interaction is believed to be dominant. Similar zonal circulation cells have been observed around the global equator (Flohn 1971; Newell 1979). As indicated by previous numerical modelings (Chervin and Druyan 1984; Stone and Chervin 1984), the global continentality and monsoon may contribute significantly to the global Walker circulation system. We have also seen that the land plays an important role in the Atlantic by changing the wind profile. It is conceivable that the land effect is even more important in the Indian Ocean, which has a completely different tropical climatology from both the Pacific and Atlantic. It is desirable that an explicit land model be included.

Acknowledgments. We thank Dr. D. Sun for very helpful discussions on atmospheric thermodynamics and the regulation of tropical SST in the early stage of the work. Discussions with Drs. J. Anderson, F. Bretherton, S. Hastenrath, D. Houghton, J. Kutzbach, G. Philander, J. Young, and especially K. Emanuel have led to improvements over an earlier version of the paper. The comments from six reviewers have helped to improve the representation of the manuscript significantly. This work is supported by the National Science Foundation and the National Oceanic and Atmospheric Administration.

APPENDIX

Spinup of the Coupled System

The formation and maintenance of the WCWC due to the Walker coupling can be seen in an example shown in Fig. A1, which plots the evolution of each term in the SST equations for eastern (Fig. A1a) and western

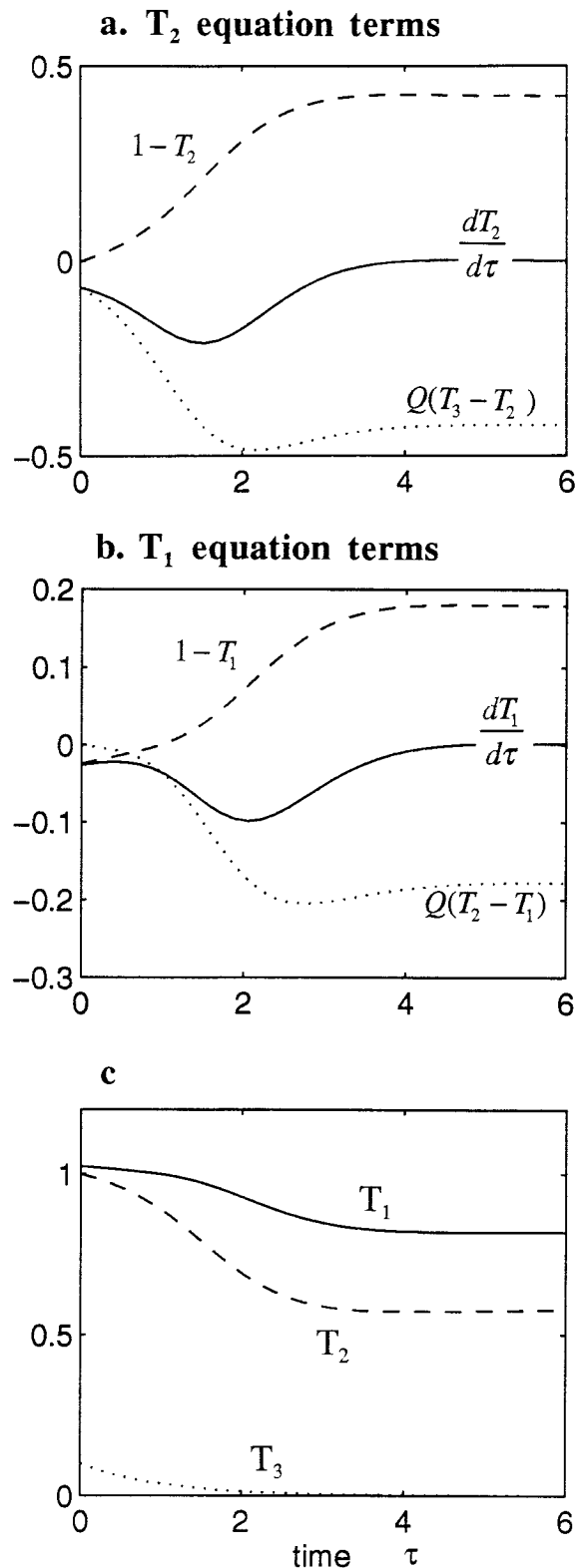


FIG. A1. Evolution processes in the simple two-box model with $m = \infty$, $\epsilon = 0$, $A_H = 0$, and $A_W = 4$. (a) Terms of the nondimensional equation for the cold tongue box T_2 . (b) The same as (a) but for the warm pool box T_1 . (c) The nondimensional temperature of each box.

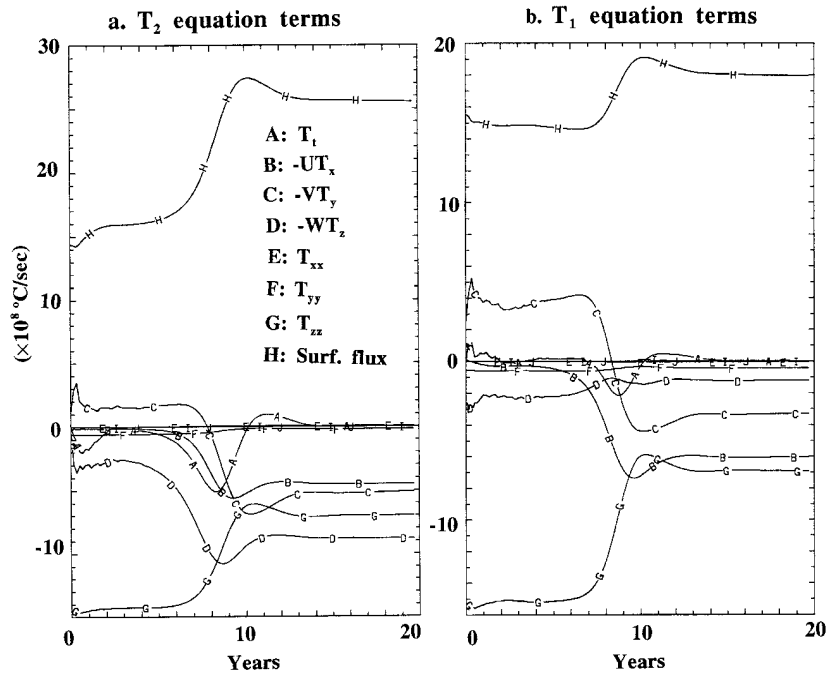


FIG. A2. The evolution of each term of the temperature equation in the (a) cold tongue and (b) warm pool areas in the upper 50 m. The first 2 yr are perturbation runs forced by a weak trade wind (0.1 dyn cm^{-2} on the equator). The coupling starts at the third year. Before the coupling, the dominant balance of the surface heat flux (H) is the vertical diffusion (G), which represents the weak model thermohaline upwelling. Within the first 6 yr after the coupling, the cold upwelling (D) intensifies dramatically in the cold tongue, which in turn causes the increase of a cold westward advection (B) in the warm pool. The reduced surface SST enhances the surface heat flux, which increases to balance the cold upwelling at about year 12. In the final state, the heat flux is mainly balanced by the cold upwelling in the cold tongue and by the cold westward advection in the warm pool. In addition, the vertical diffusion, already substantially reduced, still balances part of the surface heat flux. The unit is $10^{-8} \text{ } ^\circ\text{C s}^{-1}$. A unit heat flux ($10^{-8} \text{ } ^\circ\text{C s}^{-1}$) here can be converted to the dimensional heat flux as 2 W m^{-2} . The model setting is the same as in Fig. 6.

boxes (Fig. A1b), and the SSTs (Fig. A1c). During the initial stage (say, $\tau < 1$), the SST is cooled first in the east (Fig. A1c) because the upwelling intensifies rapidly, due to the Bjerknes positive feedback, while the surface flux remains relatively weak (Fig. A1a). Later, the increase of the cold upwelling flux is slowed down because of a smaller $T_2 - T_3$ (Fig. A1c). The surface heat flux, however, continues to increase (Fig. A1a) due to the larger deviation of T_2 from the local equilibrium SST (Figs. A1a,c). This heat flux eventually balances the cold upwelling, stabilizing the SST at a finite amplitude at about $\tau = 3$. The downstream evolution in the west is similar to that in the east, except for a smaller change of T_1 and a delay of about 1 advective time.

This process can also be seen in one GCM experiment (for the case in Fig. 6b). Each term in the SST equation is shown for the cold tongue and warm pool, respectively, in Figs. A2a,b. The initial states (year 0) in both the cold tongue and the warm pool are characterized by a heat balance between the surface heat flux (curve H) and the vertical diffusive heat flux (curve G), which parameterizes the sluggish thermohaline upwelling ef-

fect in our coarse resolution model. This is the local equilibrium state with little ocean current advection. A weak perturbation wind [$0.2P(\theta)$] is imposed for the next 2 yr to generate the initial perturbation for the following coupling run. The coupling starts at the beginning of year 3. The most important feature for the onset of the WCWC occurs after the coupling for about 7 yr, with the cold upwelling (curve D) becoming dominant in the cold tongue, cooling the SST dramatically (Fig. A2a). The warm pool is cooled after 3 yr, not by the upwelling, but by the cold westward zonal advection (curve B) (Fig. A2b). The WCWC is then stabilized at about year 8 by 100% and 20% increases of the surface heat flux in the cold tongue and warm pool, respectively. The final equilibrium is achieved mainly between the surface heat fluxes and the total oceanic advection (the sum of curve B, C, and D). The diffusive heat flux is no longer dominant, although still important. In the oceanic advection, the cold upwelling is dominant in the cold tongue while the zonal westward cold advection is dominant in the warm pool. The evolution process here agrees well with the box model in Fig. A1. Furthermore,

the value of heat flux at final equilibrium is 50 W m^{-2} in the cold tongue and 35 W m^{-2} in the warm pool, respectively. These values are within the range of observed and modeled surface heat fluxes (see discussions in Gent 1991), giving us more confidence that the GCM simulation is relevant to reality.

REFERENCES

- Bjerknes, J., 1969: Atmospheric teleconnections from the equatorial Pacific. *Mon. Wea. Rev.*, **97**, 163–172.
- Bretherton, F., 1982: Ocean climate modeling. *Progress in Oceanography*, Vol. 11, Pergamon Press, 93–129.
- Chervin, R. M., and L. M. Druyvan, 1984: The influence of ocean surface temperature gradient and continentality on the Walker circulation. Part I: Prescribed tropical changes. *Mon. Wea. Rev.*, **112**, 1510–1523.
- Clement, A. C., R. Seager, M. A. Cane, and S. E. Zebiak, 1996: An ocean dynamical thermostat. *J. Climate*, **9**, 2190–2196.
- CLIMAP Project Members, 1976: The surface of ice-age earth. *Science*, **191**, 1131–1144.
- Dijkstra, H. A., and J. D. Neelin, 1995: Ocean–atmosphere interaction and the tropical climatology. Part II: Why the Pacific cold tongue is in the east. *J. Climate*, **8**, 1343–1359.
- Fine, R. A., J. L. Reid, and H. G. Ostlund, 1981: Circulation of tritium in the Pacific Ocean. *J. Phys. Oceanogr.*, **11**, 3–14.
- , W. H. Peterson, and H. G. Ostlund, 1987: The penetration of tritium into the tropical Pacific. *J. Phys. Oceanogr.*, **17**, 553–564.
- Flohn, H., 1971: Tropical circulation patterns. *Bonner Meteor. Abhandl.*, **15**, 1–55.
- Fu, R., A. D. Del Genio, W. B. Rossow, and W. T. Liu, 1992: Cirrus-cloud thermostat for tropical sea surface temperature tested using satellite data. *Nature*, **358**, 394–397.
- Gent, P., 1991: The heat budget of the TOGA–COARE domain in an ocean model. *J. Geophys. Res.*, **96**, 3323–3330.
- Haney, R. H., 1971: Surface thermal boundary conditions for ocean circulation models. *J. Phys. Oceanogr.*, **1**, 241–248.
- Hartmann, D., and M. Michelsen, 1993: Large-scale effects on the regulation of tropical sea surface temperature. *J. Climate*, **6**, 2049–2062.
- Klinger, B., 1996: A kinematic model of wind-driven meridional heat transport. *J. Phys. Oceanogr.*, **26**, 131–135.
- Knutson, T. R., and S. Manabe, 1995: Time-mean response over the tropical Pacific to increased CO_2 in a coupled ocean–atmosphere model. *J. Climate*, **8**, 2181–2199.
- Latif, M., A. Sterl, E. Maier-Reimer, and M. M. Junge, 1993: Climate variability in a coupled GCM. Part I: The tropical Pacific. *J. Climate*, **6**, 5–21.
- Lau, N.-G., and M. J. Nath, 1996: The role of the “atmospheric bridge” in linking tropical Pacific ENSO events to extratropical SST anomalies. *J. Climate*, **9**, 2036–2057.
- Liu, Z., 1994: A simple model of the mass exchange between the subtropical and tropical ocean. *J. Phys. Oceanogr.*, **24**, 1153–1165.
- , and S. G. H. Philander, 1995: How different wind patterns affect the tropical–subtropical thermocline circulation in the upper ocean. *J. Phys. Oceanogr.*, **25**, 449–462.
- , —, and R. Pacanowski, 1994: A GCM study of tropical–subtropical upper-ocean mass exchange. *J. Phys. Oceanogr.*, **24**, 2606–2623.
- McCreary, J., and P. Lu, 1994: Interaction between the subtropical and equatorial ocean circulation: The subtropical cell. *J. Phys. Oceanogr.*, **24**, 466–497.
- McWilliams, J., and P. Gent, 1978: A coupled air and sea model for the tropical Pacific. *J. Atmos. Sci.*, **35**, 962–989.
- Mechoso, C. R., and Coauthors, 1995: The seasonal cycle over the tropical Pacific in coupled ocean–atmosphere general circulation models. *Mon. Wea. Rev.*, **123**, 2825–2838.
- Meehl, G. A., and W. M. Washington, 1996: El Niño-like climate change in a model with increased atmospheric CO_2 concentrations. *Nature*, **382**, 56–60.
- Moore, M. A., 1995: Tropical interannual variability in a global coupled GCM: Sensitivity to mean climate state. *J. Climate*, **8**, 807–828.
- Neelin, J., 1991: The slow sea surface temperature mode and the fast-wave limit: Analytical theory for tropical interannual oscillations and experiments in a hybrid coupled model. *J. Atmos. Sci.*, **48**, 584–606.
- , and H. A. Dijkstra, 1995: Ocean–atmosphere interaction and the tropical climatology. Part I: The dangers of flux correction. *J. Climate*, **8**, 1325–1342.
- , M. Latif, and F. F. Jin, 1994: Dynamics of coupled ocean–atmosphere models: The tropical problem. *Annu. Rev. Fluid Mech.*, **26**, 617.
- Newell, R. E., 1979: Climate and the ocean. *Amer. Sci.*, **67**, 405–416.
- Pedlosky, J., 1987: An inertial theory of the equatorial undercurrent. *J. Phys. Oceanogr.*, **17**, 1978–1985.
- Philander, S. G. H., 1990: *El Niño, La Niña, and the Southern Oscillation*. Academic Press, 293 pp.
- Pierrehumbert, R. T., 1995: Thermostats, radiator fins, and the local runaway greenhouse. *J. Atmos. Sci.*, **52**, 1784–1806.
- Ramanathan, V., and W. Collins, 1991: Thermodynamic regulation of ocean warming by cirrus clouds deduced from observations of the 1987 El Niña. *Nature*, **351**, 27–32.
- Seager, R., and R. Murtugudde, 1997: Ocean dynamics, thermocline adjustment, and regulation of tropical SST. *J. Climate*, **10**, 521–534.
- Stone, P. H., and R. M. Chervin, 1984: The influence of ocean surface temperature gradient and continentality on the Walker circulation. Part II: Prescribed global changes. *Mon. Wea. Rev.*, **112**, 1524–1534.
- Sun, D., and Z. Liu, 1996: Dynamic ocean–atmosphere coupling: A thermostat for the Tropics. *Science*, **272**, 1148–1150.
- Toggweiler, R., K. Dixon, and W. S. Broecker, 1989: The Peru upwelling and the ventilation of the South Pacific thermocline. *J. Geophys. Res.*, **95**, 20 467–20 497.
- Tsuchiya, M., R. Lukas, R. A. Fine, E. Firing, and E. Lindstorm, 1989: Source waters of the Pacific equatorial undercurrent. *Progress in Oceanography*, Vol. 23, Pergamon Press, 101–147.
- Waliser, D., 1996: Formation and limiting mechanisms for very high sea surface temperature: Linking the dynamics and thermodynamics. *J. Climate*, **9**, 161–188.
- Wallace, J. M., 1992: Effect of deep convection on the regulation of tropical sea surface temperature. *Nature*, **357**, 230–231.
- Wang, X., P. H. Stone, and J. Marotzke, 1995: Poleward heat transport in a barotropic ocean model. *J. Phys. Oceanogr.*, **25**, 256–265.